

Brief Papers

Adaptive Neural Network Control of Hard Disk Drives With Hysteresis Friction Nonlinearity

Phyo Phyo San, *Student Member, IEEE*, Beibei Ren, *Student Member, IEEE*, Shuzhi Sam Ge, *Fellow, IEEE*, Tong Heng Lee, *Member, IEEE*, and Jin-Kun Liu

Abstract—In this brief, an adaptive neural network (NN) friction compensator is presented for servo control of hard disk drives (HDDs). The existence of the hysteresis friction nonlinearity from pivot bearing, which is represented as the LuGre hysteresis friction model here, increases the position error signal of read-write head and deteriorates the performance of HDD servo systems. To compensate for the effect of the hysteresis friction nonlinearity, NN is adopted to approximate its unknown bounding function. With the proposed control, all the closed-loop signals are ensured to be bounded while the tracking error converges into a neighborhood of zero. Comprehensive comparisons between the conventional proportional-integral-derivative control (without friction compensator) and the proposed adaptive NN control (with friction compensator) are provided in experiment results. It is shown that the proposed control can mitigate the effect of the hysteresis friction nonlinearity and improve the track seeking performance.

Index Terms—Adaptive control, hard disk drive (HDD), hysteresis friction compensation, neural networks (NNs), pivot nonlinearity.

I. INTRODUCTION

WITH portable applications becoming more significant, there has been a corresponding increase in demand for smaller hard disk drive (HDD) with increasingly large data storage capacity. Fig. 1 shows a simple illustration of a typical HDD servo system with voice coil motor (VCM) actuator. The read/write (R/W) head is mounted on a VCM actuator assembly which is supported by a pivot cartridge consisting of a pair of preloaded ball bearings as shown in Fig. 2. The R/W head positioning is controlled by a closed-loop servo system where the actuator movement is driven by a VCM. The friction in the actuator pivot bearing significantly deteriorates the performances of HDD servo systems especially in small form factor HDDs. The residual errors caused by the friction

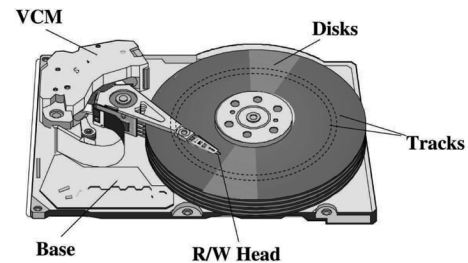


Fig. 1. Overview of an HDD system.

make head positioning servo systems difficult to maintain the R/W head over the narrower track center. The mitigation of the friction is an ongoing issue since it becomes one of challenges to design hard disk drive servo systems for small HDDs. This paper mainly focus on the compensation of the hysteresis friction nonlinearity in the actuator pivot bearing. More specifically, we will develop compensation algorithms by the use of good approximation properties of neural network (NN) and investigate the improvements in settling time and positioning error signal as well.

In order to capture the effects of pivot bearing friction in the servo control performance, various dynamic friction models have been investigated in many research works. In [1], a time-domain stick-slip friction model was proposed for representing the pivot friction. The behavior of hysteresis friction torque of pivot bearing in HDD applications was investigated in [2]. The fuzzy logic model was obtained to approximate the pivot hysteresis nonlinearity in [3]. Different models such as preload plus two-slope model and hysteretic two-slope model were studied in time domain [4] and frequency domain [5], respectively. In [6], the pivot nonlinearity in HDD was modeled as a simplified Dahl model. A dynamic pivot friction model structure was proposed which allows accurate modeling both the sliding and the presliding regimes in [7]. In [8], the LuGre friction model was introduced to capture all the static and dynamic characteristics of hysteresis friction nonlinearity. An excellent survey on friction models has been carried out in [9].

Based on the above models, many control techniques have been proposed for compensation of hysteresis friction nonlinearity in the literature. In [1], a discrete-time disturbance observer was incorporated into the conventional state feedback controller to compensate for the pivot friction nonlinearity. In [3], the fuzzy actuator pivot model was augmented into a servo design to handle pivot nonlinearity by using it as a disturbance observer. In [6], a nonlinear compensator was designed for

Manuscript received September 11, 2008; revised May 05, 2009. Manuscript received in final form January 17, 2010. First published February 17, 2010; current version published February 23, 2011. Recommended by Associate Editor G. Guo. This work was supported in part by A*STAR SERC Singapore under Grant 052 101 0097.

P. P. San, B. Ren, S. S. Ge, and T. H. Lee are with the Department of Electrical and Computer Engineering, National University of Singapore, 117576, Singapore (e-mail: elepps@nus.edu.sg; renbeibei@nus.edu.sg; samge@nus.edu.sg; eleleeth@nus.edu.sg).

J.-K. Liu is with the School of Automation Science and Electrical Engineering, Beijing University of Aeronautics and Astronautics, Beijing 100083, P. R. China (e-mail: ljk@dept3.buaa.edu.cn).

Color versions of one or more of the figures in this paper are available online at <http://ieeexplore.ieee.org>.

Digital Object Identifier 10.1109/TCST.2010.2041233

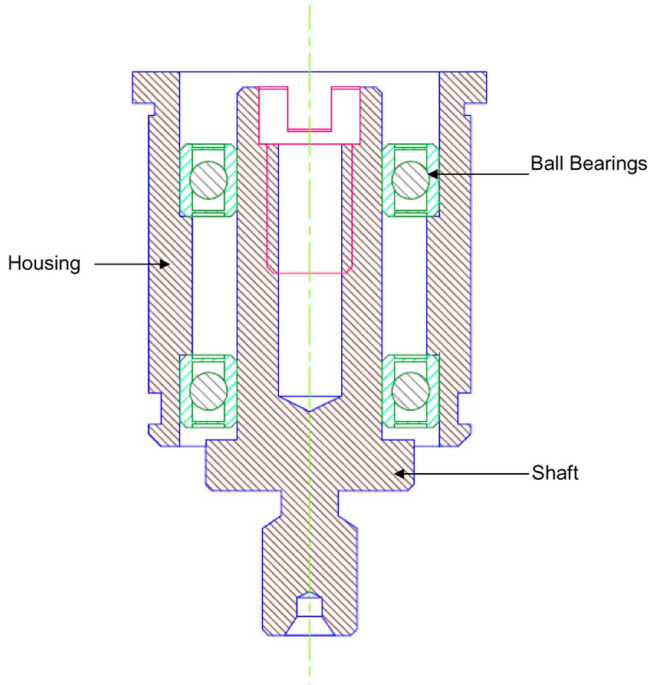


Fig. 2. Pivot bearing in HDDs.

compensation of Dahl pivot hysteresis friction nonlinearity. In [7], model-based friction compensator was proposed to improve the servo performance with additional sensor. In [10], a servo system was designed using an enhanced composite nonlinear feedback (CNF) control technique with a simple friction and nonlinearity compensation scheme. To eliminate the effect of pivot friction nonlinearity, the compensator was designed by the use of an accelerometer in [11]. Adaptive wavelet neural network control with hysteresis estimation was proposed in [12] in order to improve the control performance of a piezo-positioning mechanism. Due to the capabilities of universal approximation, learning and adaption, parallel distributed structures of neural network, it has been specified as a suitable candidature for friction modeling and adaptive control design for friction compensation. On the basis of our previous works [13]–[15], an adaptive NN friction compensator has been proposed in this paper for HDD system subject to the pivot bearing hysteresis friction nonlinearity. We can show that the proposed adaptive NN control not only reduces the effect of hysteresis friction nonlinearity, but also improves settling performance and tracking accuracy.

II. PROBLEM FORMULATION AND PRELIMINARIES

Throughout this paper, $\tilde{(\cdot)} = (\hat{\cdot}) - (\cdot)$; $\|\cdot\|$ denotes the 2-norm; $\lambda_{\min}(\cdot)$ and $\lambda_{\max}(\cdot)$ denote the smallest and largest eigenvalues of a square matrix (\cdot) , respectively.

Consider the following VCM actuator dynamics with the hysteresis friction nonlinearity:

$$m\ddot{x} + h(x, \dot{x}) + d(t) = u \quad (1)$$

where m is an unknown system constant, which models the system inertial mass; x , \dot{x} , and \ddot{x} are the position, velocity and acceleration of VCM actuator R/W head tip, respectively; $d(t)$ is the external disturbance; u is the control input; and $h(x, \dot{x})$

is the bearing hysteresis friction of actuator pivot, which is represented as a LuGre friction model consisting of stiffness and viscous friction behaviors as follows [8], [9]:

$$h = \sigma_0 z + \sigma_1 \dot{z} + \sigma_2 \dot{x} \quad (2)$$

$$\dot{z} = \dot{x} - \alpha(\dot{x})|\dot{x}|z \quad (3)$$

$$\alpha(\dot{x}) = \frac{\sigma_0}{f_c + (f_s - f_c)e^{-(\dot{x}/\dot{x}_s)^2}} \quad (4)$$

where z denotes an unmeasurable internal state of the friction model; σ_0 , σ_1 , and σ_2 are the hysteresis friction force parameters that can be physically explained as the stiffness of bristles, damping coefficient, and viscous coefficient; f_c , f_s , and \dot{x}_s are the Coulomb friction, static friction and Stribeck velocity, respectively; and the nonlinear friction characteristic function $\alpha(\dot{x})$ is a bounded positive function which can be chosen to describe different friction effects.

Remark 1: Note that there are no terms which explicitly account for the position dependence of the hysteresis friction force in the above model (2)–(4). However, there may exist some applications where the function $\alpha(\cdot)$ in the LuGre model also depends on the actual position, or on a more complex combination of position and velocity. Therefore, we assume that $\alpha(x, \dot{x})$ is an upper and lower bounded positive smooth function of x and \dot{x} , and consider the LuGre model in the following form:

$$h = \sigma_0 z + \sigma_1 \dot{z} + \sigma_2 \dot{x} \quad (5)$$

$$\dot{z} = \dot{x} - \alpha(x, \dot{x})|\dot{x}|z. \quad (6)$$

Remark 2: Fig. 3 shows that the dynamic (1)–(4) can indeed generate the hysteresis friction nonlinearity curve, where the parameters are chosen as $\sigma_0 = 10^5$, $\sigma_1 = \sqrt{10^5}$, $\sigma_2 = 0.4$, $f_c = 1$, $f_s = 1.5$, $\dot{x}_s = 0.001$, $m = 1$, and the input signal $u(t) = 0.013 \sin(180\pi t)$. Different choices of parameters can result in different hysteresis friction nonlinearity curve shapes. Recognizing the very fact that realistic accurate hysteresis friction nonlinearity model building or parameter identification might be more difficult or complicated in practice than controller design, we adopt neural networks in control design to handle the hysteresis nonlinearity and mitigate its effect on the tracking performance.

The control objective is to ensure that the position of the VCM actuator R/W head tip x follows the specified desired trajectory x_d to a small neighborhood of zero.

Assumption 1: The desired trajectories x_d and its first and second derivatives, \dot{x}_d and \ddot{x}_d , are bounded and continuous signals.

Assumption 2: The external disturbance $d(t)$ satisfies the following condition:

$$|d(t)| \leq d^*$$

where d^* is an unknown positive constant.

Assumption 3: There exist positive constants α_{\min} and α_{\max} such that $0 < \alpha_{\min} \leq \alpha(x, \dot{x}) \leq \alpha_{\max}$, $\forall (x, \dot{x}) \in R^2$.

Remark 3: According to (4) and Remark 1, Assumption 3 is valid.

Lemma 1: [8] Noting Assumption 3, if $|z(0)| \leq 1/\alpha_{\min}$, then $|z(t)| \leq 1/\alpha_{\min}$, $\forall t \geq 0$.

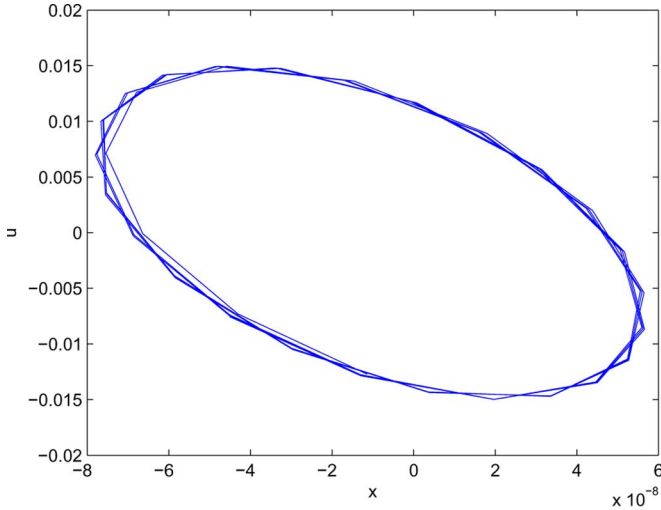


Fig. 3. Hysteresis friction curves given by dynamic models (1)–(4).

III. CONTROL DESIGN AND MAIN RESULTS

Define the tracking error e and the filtered tracking error r as follows:

$$e = x - x_d, \quad r = \dot{e} + \lambda e \quad (7)$$

where $\lambda > 0$ is a design parameter.

Define the reference velocity and acceleration signals as follows:

$$\dot{x}_r = \dot{x}_d - \lambda e, \quad \ddot{x}_r = \ddot{x}_d - \lambda \dot{e}. \quad (8)$$

Substituting (6) into (5), we obtain

$$h = \sigma \dot{x} + h_z(x, \dot{x}, z) \quad (9)$$

where $\sigma = \sigma_1 + \sigma_2$, and $h_z(x, \dot{x}, z) = \sigma_0 z - \sigma_1 \alpha(x, \dot{x}) |\dot{x}| z$, which depends on z .

From Lemma 1, we know that h_z is bounded by

$$\begin{aligned} |h_z(x, \dot{x}, z)| &= |(\sigma_0 - \sigma_1 \alpha(x, \dot{x}) |\dot{x}|) z(t)| \\ &\leq \frac{\sigma_0 + \sigma_1 \alpha(x, \dot{x}) |\dot{x}|}{\alpha_{\min}} = \bar{h}_z(x, \dot{x}) \end{aligned} \quad (10)$$

where $\bar{h}_z(x, \dot{x})$ is the bounding function of $h_z(x, \dot{x}, z)$ and is independent of the unmeasurable internal state z .

Remark 4: From (9) and (10), we know that the dynamic hysteresis friction model in (9) can be separated into two parts: 1) the term $\sigma \dot{x}$ with unknown constant coefficient and 2) the term $h_z(x, \dot{x}, z)$ which is a function of the unmeasurable internal state $z(t)$ and is bounded by a function which is independent of $z(t)$.

Then, we use radial basis function neural network (RBFNN) in [16] and [17] to approximate the unknown bounding function $\bar{h}_z(x, \dot{x})$ as

$$\bar{h}_z(x, \dot{x}) = W^{*T} S(x, \dot{x}) + \epsilon(x, \dot{x}) \quad (11)$$

where (x, \dot{x}) are the NN input signals, $W^* \in R^l$ is the optimal weight vector with the node number $l > 1$, $S(x, \dot{x}) = [s_1(x, \dot{x}), \dots, s_l(x, \dot{x})]^T$, with $s_i(x, \dot{x})$ being chosen as the commonly used Gaussian radial basis functions, and $\epsilon(x, \dot{x})$ is the NN approximation error, which satisfies

$|\epsilon(x, \dot{x})| \leq \epsilon^*$, $\forall (x, \dot{x}) \in \Omega \subset R^2$, with a compact set Ω and a positive constant ϵ^* . Since the ideal weights W^* are unknown, let \hat{W} be the estimates of W^* , and the weight estimation errors $\tilde{W} = \hat{W} - W^*$.

Let us consider the following quadratic function $V_r = 1/2mr^2$. According to (1), (7)–(11), the derivative of V_r can be written as

$$\dot{V}_r \leq r[u - \sigma \dot{x} - m\ddot{x}_r] + |r| [W^{*T} S(x, \dot{x}) + \phi] \quad (12)$$

where $\phi = \epsilon^* + d^*$. Consider the following control:

$$u = -kr + \hat{\sigma} \dot{x} + \hat{m} \ddot{x}_r - \hat{W}^T S(x, \dot{x}) \text{sgn}(r) - \hat{\phi} \text{sgn}(r) \quad (13)$$

where constant $k > 0$, $\hat{\sigma}$, \hat{m} , and $\hat{\phi}$ are the estimates of unknown parameters σ , m , and ϕ , respectively.

Substituting (13) into (12) leads to

$$\dot{V}_r \leq -kr^2 + \tilde{\sigma} \dot{x} r + \tilde{m} \ddot{x}_r r - \tilde{W}^T S(x, \dot{x}) |r| - \tilde{\phi} |r|. \quad (14)$$

Theorem 1: Consider the closed-loop system consisting of system (1) with dynamic hysteresis friction given by (5) and (6), and the control law (13). If the Assumptions 1–3 are satisfied and the parameters $\hat{\sigma}$, \hat{m} , $\hat{\phi}$, and NN weight \hat{W} are updated by

$$\dot{\hat{\sigma}} = -k_\sigma (\dot{x} r + \sigma_\sigma \hat{\sigma}) \quad (15)$$

$$\dot{\hat{m}} = -k_m (\ddot{x}_r r + \sigma_m \hat{m}) \quad (16)$$

$$\dot{\hat{\phi}} = k_\phi (|r| - \sigma_\phi \hat{\phi}) \quad (17)$$

$$\dot{\hat{W}} = \Gamma [S(x, \dot{x}) |r| - \sigma_w \hat{W}] \quad (18)$$

where k_σ , k_m , k_ϕ , σ_σ , σ_m , σ_ϕ , and σ_w are positive design constant parameters, $\Gamma = \Gamma^T > 0$ is a dimensionally compatible constant matrix, then given any initial compact set defined by

$$\Omega_0 = \left\{ x(0), x_d(0), \hat{\theta}(0), \hat{m}(0), \hat{\phi}(0), \hat{W}(0) | x(0), \hat{\theta}(0), \hat{m}(0), \hat{\phi}(0), \hat{W}(0) \text{ are chosen finite, } x_d(0) \in \Omega_d \right\}.$$

1) Uniform Boundedness (UB)

All the closed-loop signals will be remained in a compact set which is given by

$$\begin{aligned} \Omega &= \left\{ e, x, \hat{\sigma}, \hat{m}, \hat{\phi}, \hat{W} \right\} \\ |e| &\leq |e(0)| + \frac{1}{\lambda} \sqrt{\frac{2V(0) + \frac{2c_2}{c_1}}{m}} |x| \\ &\leq \max_{[0, t]} |x_d| + |e(0)| + \frac{1}{\lambda} \sqrt{\frac{2V(0) + \frac{2c_2}{c_1}}{m}}, \\ |\hat{\sigma}| &\leq |\sigma| + \sqrt{\left(2V(0) + \frac{2c_2}{c_1}\right) k_\sigma}, \\ |\hat{m}| &\leq |m| + \sqrt{\left(2V(0) + \frac{2c_2}{c_1}\right) k_m}, \\ |\hat{\phi}| &\leq |\phi| + \sqrt{\left(2V(0) + \frac{2c_2}{c_1}\right) k_\phi}, \\ \|\hat{W}\| &\leq \|W^*\| + \sqrt{\frac{2V(0) + \frac{2c_2}{c_1}}{\lambda_{\min}(\Gamma^{-1})}}. \end{aligned}$$

2) Uniformly Ultimate Boundedness (UUB)

All the closed-loop signals will eventually converge to the compact sets which is defined by

$$\Omega_s = \left\{ e, x, \hat{\sigma}, \hat{m}, \hat{\phi}, \hat{W} \mid \lim_{t \rightarrow \infty} |e| = \frac{1}{\lambda} \sqrt{\frac{2c_2}{mc_1}}, \right. \\ \lim_{t \rightarrow \infty} |x| = \max_{[0,t]} |x_d| + \frac{1}{\lambda} \sqrt{\frac{2c_2}{mc_1}}, \\ \lim_{t \rightarrow \infty} |\hat{\sigma}| = |\sigma| + \sqrt{\frac{2c_2 k_\sigma}{c_1}}, \\ \lim_{t \rightarrow \infty} |\hat{m}| = |m| + \sqrt{\frac{2c_2 k_m}{c_1}}, \\ \lim_{t \rightarrow \infty} |\hat{\phi}| = |\phi| + \sqrt{\frac{2c_2 k_\phi}{c_1}}, \\ \left. \lim_{t \rightarrow \infty} \|\hat{W}\| = \|W^*\| + \sqrt{\frac{2c_2}{\lambda_{\min}(\Gamma^{-1})c_1}} \right\}.$$

In particular, the tracking error will converge to a neighborhood of zero by adjusting some control design parameters.

Proof: Consider the following Lyapunov function candidate:

$$V = V_r + \frac{1}{2k_\sigma} \tilde{\sigma}^2 + \frac{1}{2k_m} \tilde{m}^2 + \frac{1}{2k_\phi} \tilde{\phi}^2 + \frac{1}{2} \tilde{W}^T \Gamma^{-1} \tilde{W}. \quad (19)$$

Its derivative along (14)–(18) is

$$\dot{V} \leq -kr^2 - \sigma_\sigma \tilde{\sigma} \hat{\sigma} - \sigma_m \tilde{m} \hat{m} - \sigma_\phi \tilde{\phi} \hat{\phi} - \sigma_w \tilde{W} \hat{W}. \quad (20)$$

By completion of squares, the following inequalities hold:

$$-\sigma_\sigma \tilde{\sigma} \hat{\sigma} \leq -\frac{\sigma_\sigma}{2} \tilde{\sigma}^2 + \frac{\sigma_\sigma}{2} \sigma^2 \quad (21)$$

$$-\sigma_m \tilde{m} \hat{m} \leq -\frac{\sigma_m}{2} \tilde{m}^2 + \frac{\sigma_m}{2} m^2 \quad (22)$$

$$-\sigma_\phi \tilde{\phi} \hat{\phi} \leq -\frac{\sigma_\phi}{2} \tilde{\phi}^2 + \frac{\sigma_\phi}{2} \phi^2 \quad (23)$$

$$-\sigma_w \tilde{W}^T \hat{W} \leq -\frac{\sigma_w}{2} \|\tilde{W}\|^2 + \frac{\sigma_w}{2} \|W^*\|^2. \quad (24)$$

Substituting (21)–(24) into (20), we have the following equations:

$$\dot{V} \leq -c_1 V + c_2 \quad (25)$$

where

$$c_1 = \min \left\{ 2k, \sigma_\sigma k_\sigma, \sigma_m k_m, \sigma_\phi k_\phi, \frac{\sigma_w}{\lambda_{\max}(\Gamma^{-1})} \right\} \\ c_2 = \frac{\sigma_\sigma}{2} \sigma^2 + \frac{\sigma_m}{2} m^2 + \frac{\sigma_\phi}{2} \phi^2 + \frac{\sigma_w}{2} \|W^*\|^2. \quad (26)$$

Multiplying both sides of (25) by $e^{c_1 t}$ and integrating over $[0, t]$ leads to the following equation:

$$0 \leq V(t) \leq \left[V(0) - \frac{c_2}{c_1} \right] e^{-c_1 t} + \frac{c_2}{c_1} \quad (27)$$

where

$$V(0) = \frac{1}{2} m r^2(0) + \frac{1}{2k_\sigma} \tilde{\sigma}^2(0) + \frac{1}{2k_m} \tilde{m}^2(0) \\ + \frac{1}{2k_\phi} \tilde{\phi}^2(0) + \frac{1}{2} \tilde{W}^T(0) \Gamma^{-1} \tilde{W}(0).$$

1) Uniform Boundedness (UB)

From (27), we have

$$0 \leq V(t) \leq \left[V(0) - \frac{c_2}{c_1} \right] e^{-c_1 t} + \frac{c_2}{c_1} \leq V(0) + \frac{c_2}{c_1}. \quad (28)$$

From (19) and (28), we have

$$|\hat{\sigma}| \leq |\sigma| + \sqrt{\left(2V(0) + \frac{2c_2}{c_1} \right) k_\sigma} \\ |\hat{m}| \leq |m| + \sqrt{\left(2V(0) + \frac{2c_2}{c_1} \right) k_m} \\ |\hat{\phi}| \leq |\phi| + \sqrt{\left(2V(0) + \frac{2c_2}{c_1} \right) k_\phi} \\ \|\hat{W}\| \leq \|W^*\| + \sqrt{\frac{2V(0) + \frac{2c_2}{c_1}}{\lambda_{\min}(\Gamma^{-1})}}.$$

From the definition of r in (7), we have that $\dot{e} = \lambda e + r$. Solving this equation results in

$$e = e^{-\lambda t} e(0) + \int_0^t e^{-\lambda(t-\tau)} |r| d\tau. \quad (29)$$

Therefore, the following equation is obtained:

$$|e| \leq |e(0)| + \frac{1}{\lambda} \sqrt{\frac{2V(0) + \frac{2c_2}{c_1}}{m}}. \quad (30)$$

From (7), we have

$$|x| \leq \max_{[0,t]} |x_d| + |e(0)| + \frac{1}{\lambda} \sqrt{\frac{2V(0) + \frac{2c_2}{c_1}}{m}}. \quad (31)$$

2) Uniformly Ultimate Boundedness (UUB)

Let us analyze the property of $|r|$ first. From (19) and (27), we have

$$|r| \leq \sqrt{\frac{2 \left[V(0) - \frac{c_2}{c_1} \right] e^{-c_1 t} + \frac{2c_2}{c_1}}{m}} \\ |\dot{\sigma}| \leq \sqrt{\left[2 \left(V(0) - \frac{c_2}{c_1} \right) e^{-c_1 t} + \frac{2c_2}{c_1} \right] k_\sigma}. \quad (32)$$

If $V(0) = c_2/c_1$, then $|r| \leq \sqrt{2c_2/mc_1}$, $\forall t \geq 0$. If $V(0) \neq c_2/c_1$, from (32), we can conclude that given any $\mu_r > 2c_2/mc_1$, there exists T_r , such that for any $t > T_r$, we have $|r| \leq \mu_r$, and

$$\lim_{t \rightarrow \infty} |r| = \sqrt{\frac{2c_2}{mc_1}}. \quad (33)$$

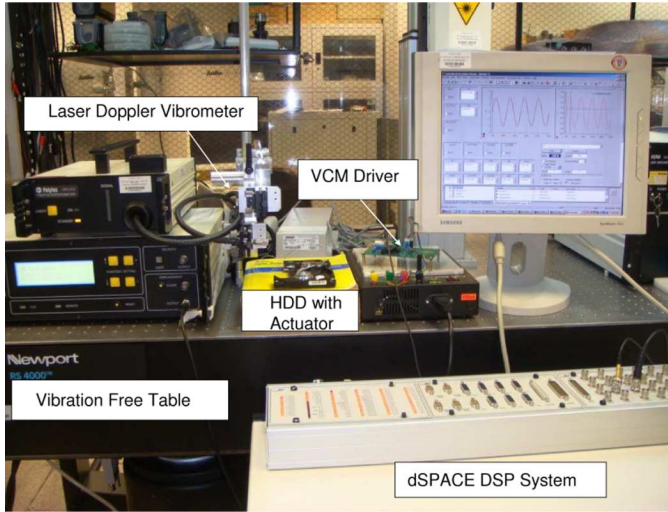


Fig. 4. Experimental setup.

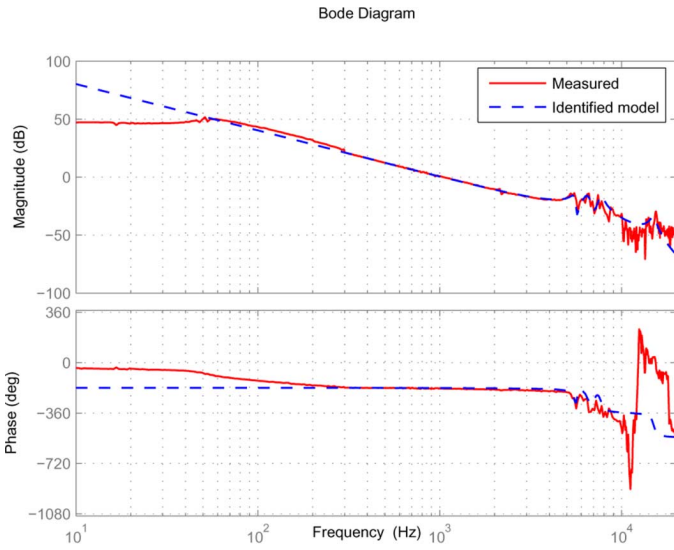


Fig. 5. Frequency response of measured and identified HDD actuator model.

From (29) and (33), we obtain that

$$\lim_{t \rightarrow \infty} |e| = \frac{1}{\lambda} \sqrt{\frac{2c_2}{mc_1}} \quad (34)$$

and

$$\lim_{t \rightarrow \infty} |x| = \max_{[0,t]} |x_d| + \frac{1}{\lambda} \sqrt{\frac{2c_2}{mc_1}}. \quad (35)$$

Similar conclusions can be made about $|\hat{\sigma}|$, $|\hat{m}|$, $|\hat{\phi}|$, $\|\hat{W}\|$ as follows:

$$\begin{aligned} \lim_{t \rightarrow \infty} |\hat{\sigma}| &= |\sigma| + \sqrt{\frac{2c_2 k_\sigma}{c_1}} \\ \lim_{t \rightarrow \infty} |\hat{m}| &= |m| + \sqrt{\frac{2c_2 k_m}{c_1}} \\ \lim_{t \rightarrow \infty} |\hat{\phi}| &= |\phi| + \sqrt{\frac{2c_2 k_\phi}{c_1}} \\ \lim_{t \rightarrow \infty} \|\hat{W}\| &= \|W^*\| + \sqrt{\frac{2c_2}{\lambda_{\min}(\Gamma^{-1})c_1}}. \end{aligned}$$

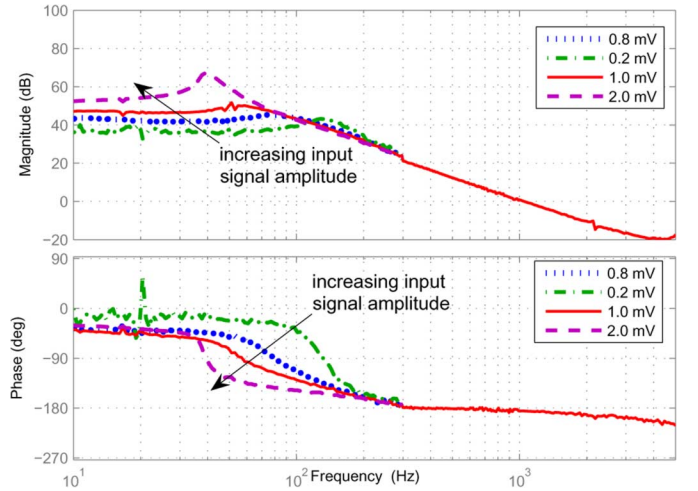


Fig. 6. Frequency responses of VCM actuator under the influence of pivot friction nonlinearity with different swept-sine input signal amplitudes at low frequency range, 10–200 Hz.

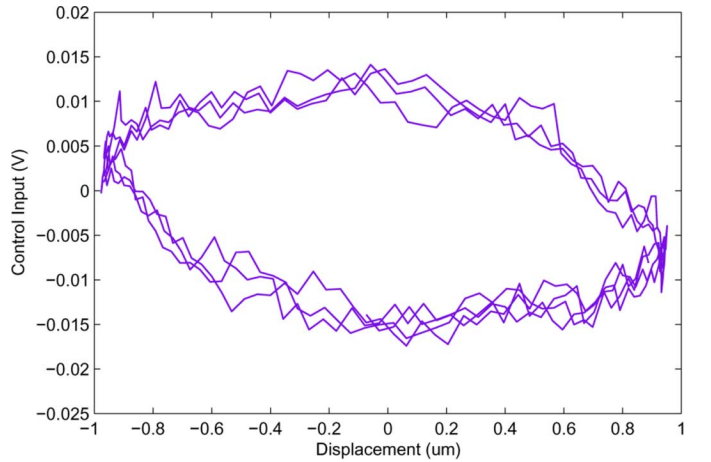


Fig. 7. Experimental pivot hysteresis friction nonlinearity curve at frequency 80 Hz.

From (34) and the definitions of c_1 and c_2 in (26), we know that the tracking error e can converge to a neighborhood of zero after increasing the parameters λ , k , k_σ , k_m , k_ϕ , $1/(\lambda_{\max}(\Gamma^{-1}))$, and decreasing σ_σ , σ_m , σ_ϕ , σ_w . ■

IV. EXPERIMENTAL STUDIES

The experiments are conducted on a dSPACE digital signal processor with a sampling time $T = 0.1$ ms as can be seen in Fig. 4. A VCM actuator from commercial 3.5-in HDD (Seagate Barracuda 7200.10) is used for the verification of proposed adaptive NN control. The HDD is partially cut off to measure the read/write head displacement of VCM actuator using the Laser-Doppler-Scanning-Vibrometer (LDV) with a resolution set to $8 \mu\text{m}/\text{V}$. The measured R/D head displacement is fed into the dSPACE digital signal processing system to generate necessary control input signals.

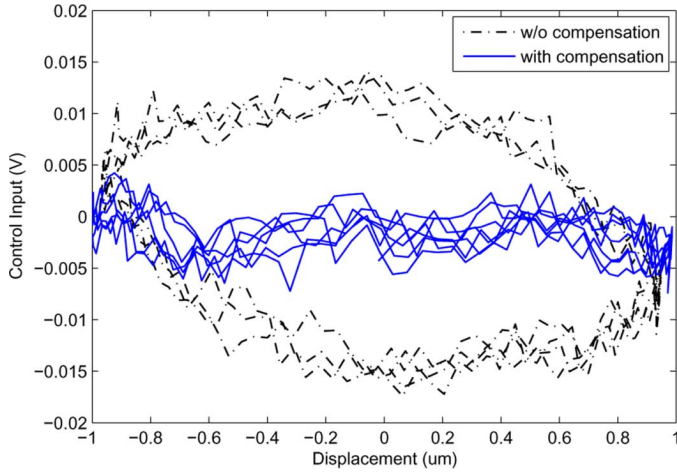


Fig. 8. Comparison results of experimental pivot hysteresis friction nonlinearity curves with and without friction compensation at frequency 80 Hz.

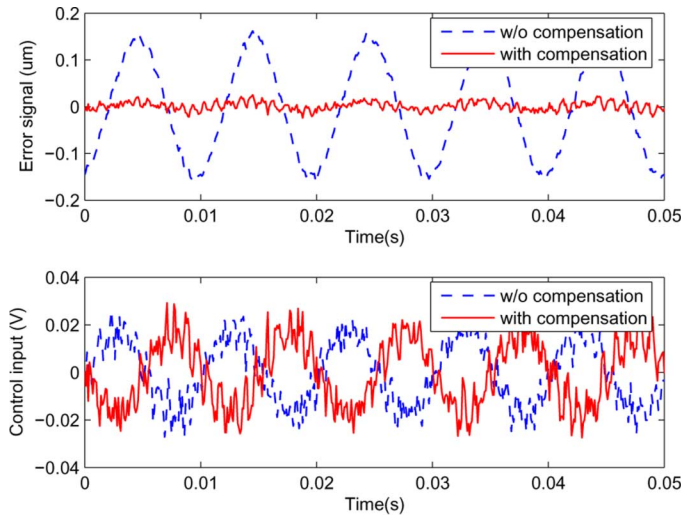


Fig. 9. Tracking error and control input signals for the desired sinusoidal trajectory with $A = 2$ and $f = 100$ Hz.

A. Modeling and Identification of HDD System

As investigated in [7] and [18], the modeling of VCM actuator in HDD system at low frequencies could be described by the integration of a double integrator with a friction model, which have been shown to be independent of each other by extensive experimental results and data analysis. Moreover, there are some high frequency resonances at high frequency range. The frequency response of VCM actuator is obtained and shown in Fig. 5 by using position feedback signal of VCM actuator measured from LDV to Dynamic Signal Analyzer (DSA-Hp 35670A).

By curve-fitting to the measured frequency response in Fig. 5, we obtain the double integrator model

$$G_P = \frac{4.0968 \times 10^7}{s^2} \quad (36)$$

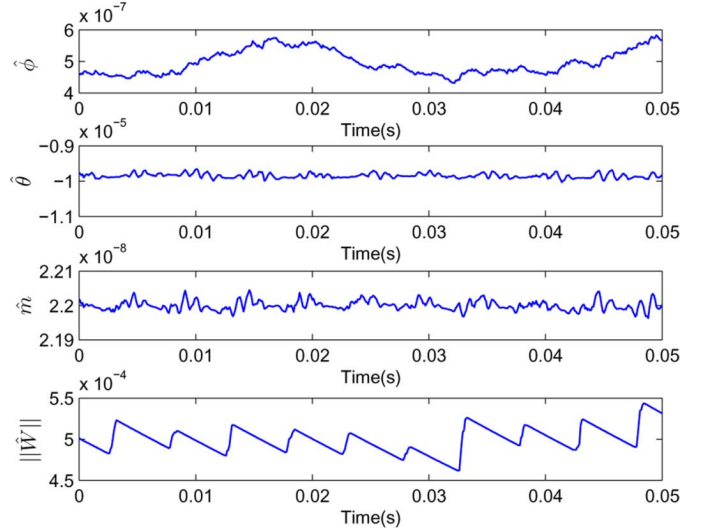


Fig. 10. Tracking error and control input signals for the desired sinusoidal trajectory with $A = 2$ and $f = 100$ Hz.

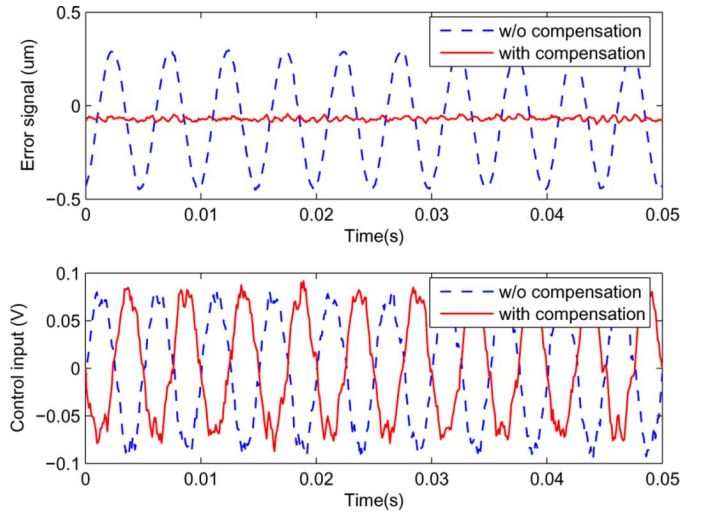


Fig. 11. Tracking error and control input signals for the desired sinusoidal trajectory with $A = 2$ and $f = 200$ Hz.

which is independent of hysteresis friction effect; and the high frequency modes at 5.5, 6.5, 7.86, 15 kHz are represented as follows:

$$G_{R1} = \frac{0.9321s^2 + 678.3s + 1.184 \times 10^9}{s^2 + 2053s + 1.184 \times 10^9} \quad (37)$$

$$G_{R2} = \frac{0.8249s^2 + 2251s + 1.665 \times 10^9}{s^2 + 3276s + 1.665 \times 10^9} \quad (38)$$

$$G_{R3} = \frac{2.431 \times 10^9}{s^2 + 2703s + 2.431 \times 10^9} \quad (39)$$

$$G_{R4} = \frac{8.383 \times 10^9}{s^2 + 5655s + 8.383 \times 10^9} \quad (40)$$

From Fig. 5, it can be seen that measured frequency responses of VCM actuator and its identified frequency responses [double integrator (36) + four high frequency modes (37)–(40)] has a close match except for the low frequency range 10–200 Hz,

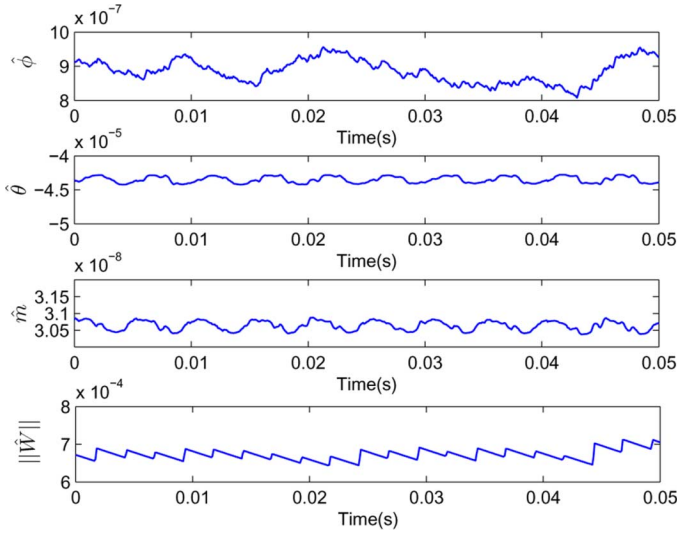


Fig. 12. Parameters adaptations for the desired sinusoidal trajectory with $A = 2$ and $f = 200$ Hz.

where the friction nonlinearity mainly exists. For high frequency resonances, they can be handled by the use of notch filters in [19] and [20]. However, in this paper, our focus is not on the high frequency resonances, but the compensation of the friction nonlinearity at low frequency components. Therefore, the implementation issues of notch filters are not considered in this paper. In the following, we focus on the compensation of friction nonlinearity problem at the low frequency range 10–200 Hz.

Since the VCM actuator in hard disk drive system has a characteristic of double integrator model, it is expected to show -40 dB/decade slope and -180° phase at the low frequency range 10–200 Hz. However, the experimentally obtained frequency response in Fig. 5 shows 0 dB/decade slope and 0° phase at low frequency range 10–200 Hz. It can be explained that the effect of friction is manifested as reduction in gain at low frequency and the reduction depends on the amplitude of the excitation signal which is used to measure the frequency response, as discussed in [7], [18], and shown in Fig. 10 with different amplitude swept-sine excitation signals. In particular, Fig. 7 shows the hysteresis friction nonlinearity curve at low frequency 80 Hz. It is consistent with the hysteresis friction curve generated by the LuGre friction model (2)–(4) in Fig. 3. Instead of conducting parameter identifications for the LuGre friction model, we adopt neural networks to approximate the unknown bounding function of the LuGre friction model as (11). Fig. 8 shows the hysteresis friction curve with and without NN compensation, which indicates that the effect of the hysteresis friction can be mitigated well by NN approximation.

B. Experiment Results

In this section, extensive implementation results are presented to demonstrate the effectiveness of proposed adaptive neural network (NN) control scheme for both sinusoidal and step responses.

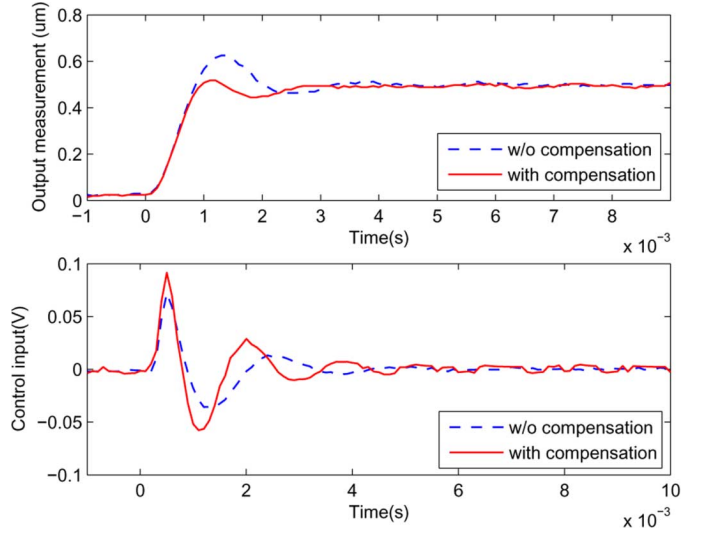


Fig. 13. Step response with amplitude $0.5 \mu\text{m}$.

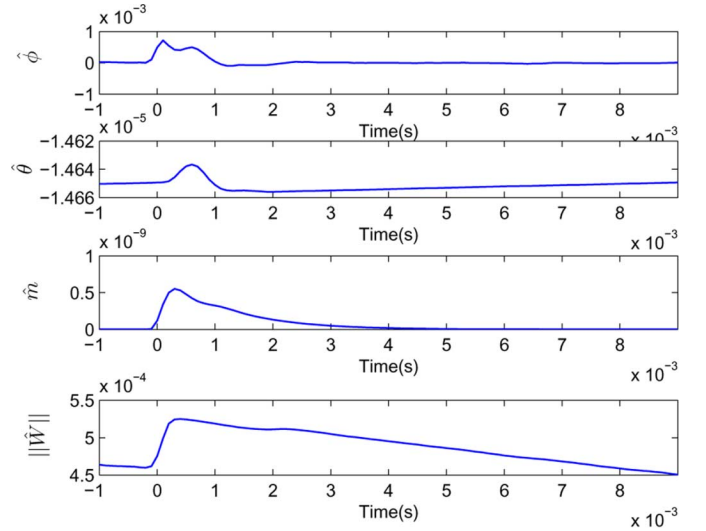


Fig. 14. Parameters adaptations for step response with amplitude $0.5 \mu\text{m}$.

First, we consider the reference signal, x_d as a sinusoidal, $x_d = A \sin(\pi ft)$, where A is the amplitude and f is the frequency. The control parameters for (13) and adaption laws (15) are chosen as: $\lambda = 595.0$, $k = 7.9 \times 10^{-15}$, $k_\sigma = 1.0 \times 10^{-9}$, $k_\phi = 1.5 \times 10^{-6}$, $k_m = 2.0 \times 10^{-14}$, $\sigma_\sigma = 1.5 \times 10^7$, $\sigma_\phi = 1.2 \times 10^7$, $\sigma_m = 4.99 \times 10^{13}$, $\Gamma = \text{diag}\{1.0\}$, $\sigma_w = 7.0 \times 10^3$. All the initial values are set to zero. Figs. 9 and 11 show that, compared with the conventional PID control (without friction compensator), our proposed adaptive NN controller (with friction compensator) can successfully reduce the tracking error to neighborhood of zero for the sinusoidal reference signal with amplitude of $2 \mu\text{m}$ and frequencies at 100 and 200 Hz, respectively, which belong to the frequency range of 10–200 Hz as shown in Fig. 10. The boundedness of the parameter estimates in the proposed adaptive neural network control are presented in Figs. 10 and 12.

Second, the step response is investigated by choosing square wave signal as the desired trajectory. Good tracking performances for a demand step of 0.5 and $5 \mu\text{m}$ are achieved as

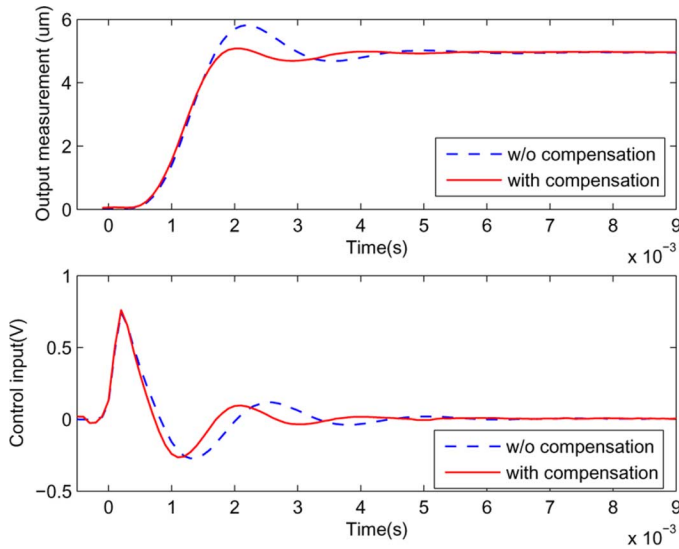


Fig. 15. Step response with amplitude $5 \mu\text{m}$.

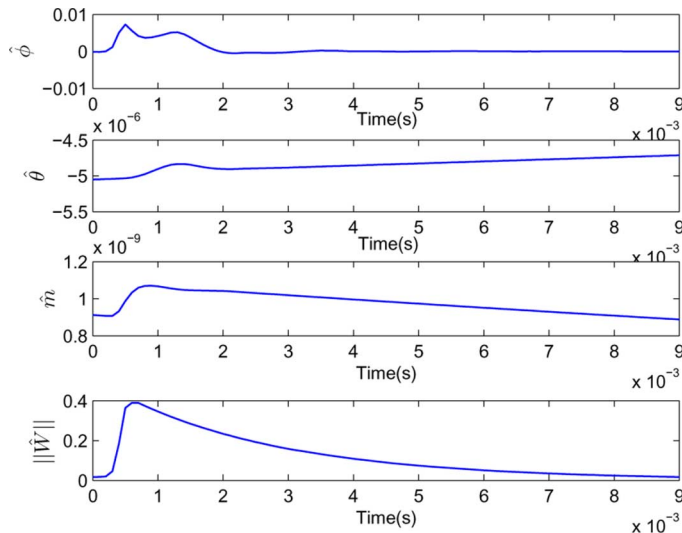


Fig. 16. Parameters adaptations for step response with amplitude $5 \mu\text{m}$.

shown in Figs. 13 and 15. Compared with the conventional PID control, the proposed adaptive NN control can decrease the overshoot and reduce the settling time performance without degrading the tracking accuracy. Figs. 14 and 16 show the boundedness of the parameter estimates.

V. CONCLUSION

In this brief, a pivot friction compensation method by the use of adaptive neural network control has been proposed. Through experiment results using a 3.5-in disk drive, it has been shown

that the proposed friction compensator can mitigate the hysteresis friction nonlinearity very well and guaranteed that the position error signal converged to a neighborhood of zero. The proposed control is simpler and easily implemented in practice.

REFERENCES

- [1] H. T. Goh, S. Weerasooriya, T. S. Low, and Y. H. Huang, "Modeling and compensation of pivot friction in a disk drive actuator," in *Proc. Amer. Control Conf.*, 1995, pp. 4141–4145.
- [2] X. Liu and J. C. Liu, "Analysis and measurement of torque hysteresis of pivot bearing in hard disk drive applications," *Tribology Int.*, vol. 32, no. 3, pp. 125–130, 1999.
- [3] T. Huang, Y. Ding, S. Weerasooriya, and T. S. Low, "Disk drive pivot nonlinearity modeling and compensation through fuzzy logic," *IEEE Trans. Magn.*, vol. 34, no. 1, pp. 30–35, Jan. 1998.
- [4] F. Wang, T. Hurst, D. Abramovitch, and G. Franklin, "Disk drive pivot nonlinearity modeling part II: Time domain," in *Proc. Amer. Control Conf.*, 1994, pp. 2604–2607.
- [5] D. Abramovitch, F. Wang, and G. Franklin, "Disk drive pivot nonlinearity modeling part I: Frequency domain," in *Proc. Amer. Control Conf.*, 1994, pp. 2600–2603.
- [6] J. Q. Gong, L. Guo, H. S. Lee, and B. Yao, "Modeling and cancellation of pivot nonlinearity in hard disk drives," *IEEE Trans. Magn.*, vol. 38, no. 5, pp. 3560–3565, Sep. 2002.
- [7] T. Yan and R. Lin, "Experimental modeling and compensation of pivot nonlinearity in hard disk drives," *IEEE Trans. Magn.*, vol. 39, no. 2, pp. 1064–1069, Mar. 2003.
- [8] C. C. de Wit, H. Olsson, K. J. Astrom, and P. Lischinsky, "A new model for control of systems with friction," *IEEE Trans. Autom. Control*, vol. 40, no. 3, pp. 419–425, Mar. 1995.
- [9] B. Armstrong-Héouvy, P. Dupont, and C. C. de Wit, "A survey of models, analysis tools and compensation methods for the control of machines with friction," *Automatica*, vol. 30, no. 7, pp. 1083–1138, 1994.
- [10] K. Peng, B. M. Chen, G. Cheng, and T. H. Lee, "Modeling and compensation of nonlinearities and friction in a micro hard disk drive servo system with nonlinear feedback control," *IEEE Trans. Control Syst. Technol.*, vol. 13, no. 5, pp. 708–721, Sep. 2005.
- [11] J. Ishikawa and M. Tomizuka, "Pivot friction compensation using an accelerometer and a disturbance observer for hard disk drives," *IEEE/ASME Trans. Mechatronics*, vol. 3, no. 3, pp. 194–201, Sep. 1998.
- [12] F. J. Lin, H. J. Shieh, and P. K. Huang, "Adaptive wavelet neural network control with hysteresis estimation for piezo-positioning mechanism," *IEEE Trans. Neural Netw.*, vol. 17, no. 2, pp. 432–444, Mar. 2006.
- [13] S. S. Ge, T. H. Lee, and S. X. Ren, "Adaptive friction compensation of servo mechanisms," *Int. J. Syst. Sci.*, vol. 32, no. 4, pp. 523–532, 2001.
- [14] G. Herrmann, S. S. Ge, and G. Guo, "Practical implementation of a neural network controller in a hard disk drive," *IEEE Trans. Control Syst. Technol.*, vol. 13, no. 1, pp. 146–154, Jan. 2005.
- [15] S. S. Ge, B. Ren, and T. H. Lee, "Hard disk drives control in mobile applications," *J. Syst. Sci. Complexity*, vol. 20, no. 2, pp. 215–224, 2007.
- [16] R. M. Sanner and J. E. Slotine, "Gaussian networks for direct adaptive control," *IEEE Trans. Neural Netw.*, vol. 3, no. 6, pp. 837–863, Nov. 1992.
- [17] S. S. Ge, C. C. Hang, T. H. Lee, and T. Zhang, *Stable Adaptive Neural Network Control*. Boston, MA: Kluwer, 2002.
- [18] B. Hredzak, F. Hong, S. S. Ge, J. Zhang, and Z. He, "Modeling and compensation of pivot nonlinearity in hard disk drives," in *Proc. 16th IEEE Int. Conf. Control Appl.*, 2007, pp. 108–113.
- [19] P. A. Weaver and R. M. Ehrlich, "The use of multirate notch filters in embedded-servo disk drives," in *Proc. Amer. Control Conf.*, 1995, pp. 4156–4160.
- [20] D. Wu, G. Guo, and T. C. Chong, "Comparative analysis on resonance compensation in HDD dual-stage actuation systems," *IEEE Trans. Ind. Electron.*, vol. 50, no. 6, pp. 1179–1186, Dec. 2003.